Self-Assembly of Fluorescent Amphipathic Borondipyrromethene Scaffoldings in Mesophases and Organogels

Franck Camerel,[†] Laure Bonardi,[†] Gilles Ulrich,[†] Loïc Charbonnière,[†] Bertrand Donnio,[‡] Cyril Bourgogne,[‡] Daniel Guillon,[‡] Pascal Retailleau,[§] and Raymond Ziessel*[,†]

Laboratoire de Chimie Moléculaire, Ecole Chimie, Polymères, Matériaux (ECPM), Université Louis Pasteur-CNRS (UMR 7509), 25 Rue Becquerel, F-67008 Strasbourg Cedex, France, Institut de Physique et Chimie des Matériaux de Strasbourg (IPCMS), Groupe des Matériaux Organiques (GMO), UMR 7504 (ULP-CNRS), 23 Rue du Loess, BP 43, F-67034 Strasbourg Cedex 2, France, and Laboratoire de Cristallochimie, ICSN−CNRS, Bât 27, 1 Avenue de la Terrasse, F-91198 Gif-sur-Yvette, France

Received May 16, 2006. Revised Manuscript Received July 27, 2006

Mesogenic scaffoldings are constructed from highly luminescent 4,4-difluoro-4-bora-3a,4a-diaza-*s*-indacene (Bodipy) linked via an amide or an ethynyl spacer to a functional amphipathic platform. A single-crystal X-ray structure of a parent methoxy compound revealed that the Bodipy fragment is almost perpendicular to the aromatic core of the functional platform and that hydrogen-bonded dimers form one-dimensional crystallographic chains through the stacking of two Bodipy residues. The functional molecules self-assemble into thermotropic and fluorescent columnar mesophases with a hexagonal symmetry as deduced from small-angle X-ray scattering. An unprecedented texture of the Bodipy mesophase was observed by fluorescence microscopy and correlates the classical texture observed by polarized optical microscopy. Molecular modeling and FT-IR strongly suggest that the driving forces for the emergence of the mesophase is the formation of a tight hydrogen-bonded network, combined with stacking of the Bodipy fragments. Besides, the tris-amide ($n = 16$), Bodipy compound proved to be an excellent gelator of nonane in particular. The resulting robust gels are highly luminescent, and transmission electron microscopy revealed that the gels are mastered through the formation of an interconnected network of fibrils. Temperature-dependent FT-IR spectroscopy shows that the amide functions are engaged in hydrogen bonds that are not disrupted above the sol−gel transition. Temperature-dependent ^{1}H, ^{11}B NMR experiments and fluorescence spectroscopy results are in line with a gelification process driven by the aggregation of the Bodipy residues into large objects by formation of *J*-aggregates.

Introduction

Numerous molecules can spontaneously organize into well-defined assemblies with special physical properties lying between those of the molecule and those of bulk material. Landmark examples of hierarchical assemblies include micelles, liposomes, microcapsules, dendrimers, colloidal particles, gels, and liquid crystalline materials.[1,2] Among these soft materials, supramolecular gels and liquid crystalline materials are of particular interest because they can respond to external stimuli like heat, electric pulse, light, and chemicals.[3] Gelation properties can also be reversibly switched in some cases by appropriate changes in pH, geometrical distortion, and oxidation state.[4−6] In addition, lyotropic gels, engineered from low molecular weight gelator and entrapped liquid-crystal frameworks, exhibit unique optical properties and dynamical functions due to cooperative network effects inside the gelator assemblies.[7] Many different types of low molecular mass gelators have been recently developed including steroid,[8] amino acids,[9] bis-urea,[10] sug-

* Corresponding author. E-mail: ziessel@chimie.u-strasbg.fr.
[†] LCM, ECPM, ULP, Strasbourg.
[‡] GMO, IPCMS, Strasbourg.
[§] ICSN, CNRS, Gif-sur-Yvette.

(1) (a) Hudson, S. D.; Jung, H.-T.; Percec, V.; Cho, W.-D.; Johansson, G.; Ungar, G.; Balagurusamy, V. S. K. *Science* **1997**, *278*, 449. (b) Kukula, H.; Schlaad, H.; Antonietti, M.; Förster, S. *J. Am. Chem. Soc.* **2002**, *124*, 1658. (c) Tedeschi, C.; Li, L.; Möhwald, H.; Spitz, C.; von Seggern, D.; Menzel, R.; Kirstein, S. *J. Am. Chem. Soc.* **2004**, *126*, 3218. (d) Li, L.; Möhwald, H. *Angew. Chem. Int. Ed.* **2004**, *43*, 360; (e) Hoeben, F. J. M.; Jonkheijm, P.; Meijer, E. W.; Schenning, A. P. H. J. *Chem. Rev.* **2005**, *105*, 1491.

(2) (a) Donnio, B.; Guillon, D.; Bruce, D. W.; Deschenaux, R. Metallomesogens. In *Comprehensive Coordination Chemistry II: From Biology to Nanotechnology*, Vol. 7; McCleverty, J. A., Meyer, T. J., Eds.; Fujita, M., Powell, A., Creutz, C., Vol. Eds.; Elsevier: Oxford, UK, 2003; Chapter 7.9, pp 357−627. (b) Terech, P.; Weiss, R. G. *Chem. Rev.* **1997**, *97*, 3133. (c) Estroff, L. A.; Hamilton, A. D. *Chem. Rev.* **2004**, *104*, 1201. (d) Xiao, S.; Myers, M.; Miao, Q.; Sanaur, S.; Pang, K.; Steigerwald, M. L.; Nuckolls, C. *Angew. Chem. Int. Ed.* **2005**, *44*, 7390. (e) Wu, J.; Li, J.; Kolb, U.; Müllen, K. *Chem. Commun.* **2006**, 48. (h) Hatano, T.; Kato, T. *Chem. Commun.* **2006**, 1277.

(3) Sangeetha, N. M.; Maitra, U. *Chem. Soc. Rev.* **2005**, *34*, 821.

(4) (a) de Jong, J. J. D.; Lucas, L. N.; Kellogg, R. M.; van Esh, J. H.; Feringa, B. L. *Science* **2004**, *304*, 278. (b) Maitra, U.; Mukhopadhyay, S.; Sarkar, A.; Rao, P.; Indi, S. S. *Angew. Chem. Int. Ed.* **2001**, *40*, 2281. (c) Sugiyasu, K.; Fujita, N.; Takeuchi, M.; Yamada, S.; Shinkai, S. *Org. Biomol. Chem.* **2003**, *1*, 895. (d) Shirakawa, M.; Fujita, N.; Tani, T.; Kaneko, K.; Shinkai, S. *Chem. Commun.* **2005**, 4149.

(5) Beck, J. B.; Rowan, S. J. *J. Am. Chem. Soc.* **2003**, *125*, 13922.

(6) Kawano, S.-I.; Fujita, N.; Shinkai, S. *J. Am. Chem. Soc.* **2004**, *126*, 8592.

(7) (a) Kato, T. *Science* **2002**, *295*, 2414. (b) Ajayaghosh, A.; George, S. J.; Praveen, V. K. *Angew. Chem. Int. Ed.* **2003**, *42*, 332. (c) Sugiyasu, K.; Fujita, N.; Shinkai, S. *Angew. Chem. Int. Ed.* **2004**, *43*, 1229. (d) Del Guerzo, A.; Olive, A. G. L.; Reichwagen, J.; Hopf, H.; Desvergne, J.-P. *J. Am. Chem. Soc.* **2005**, *127*, 17984. (e) Montalti, M.; Dolci, L. S.; Prodi, L.; Zaccheroni, N.; Stuart, M. C. A.; van Bommel, K. J. C.; Friggeri, A. *Langmuir* **2006**, *22*, 2299.

(8) Sugiyasu, K.; Fujita, N.; Shinkai, S. *Angew. Chem. Int. Ed.* **2004**, *43*, 1229.

10.1021/cm0611441 CCC: $33.50
Published on Web 09/14/2006

ars,[11] polypeptides,[12] gemini surfactants/bolaamphiphiles,[13] tripodal cholamides,[14] and bile acids.[15] The incorporation of functional subunits such as cyanostilbene,[16] bithiophene,[17] and tetrathiafulvalene[18] in the molecular framework is attracting a lot of interest due to the increase of charge-carrier mobility. Gels can also find applications in colorimetric sensing and as templates for the preparation of structured materials and in biomedical applications for the controlled release of molecules, specifically for drug delivery.[4,19]

The design of luminescent and photoresponsive gels and liquid crystals is particularly appealing due to their potential photonic applications such as OLEDs[20] and energy convectors like photovoltaic cells.[21] In recent years, gelators based on porphyrins,[22] phthalocyanines,[23] phenylenevinylenes,[24] perylenes,[25] triphenylene,[26] amphiphiles imidazoles,[27] stilbene,[28] and azo groups[29] have been reported. In particular, strong fluorescence emission was recently obtained by incorporating oxadiazoles in benzene-tricarboxamide.[30] Furthermore, anionic fluorescent hydrogels[31a] and phosphorescent organogels engineered from gold(I) complexes are particularly attractive in photoregulation and electroluminescent devices.[31b]

On the other hand, a promising class of dyes based on Bodipy derivatives, fulfilling the criteria of stability and chemical availability combined with high molar extinction coefficients, high fluorescence quantum yields, and narrow emission bandwidths,[32−34] remains completely unexplored in supramolecular gels and liquid crystalline materials. Furthermore, they exhibit strong chemical and photochemical stability in solution and in the solid state and remarkable electron-transfer properties. The optical properties are sensitive to modifications of the pyrrole core,[35] the central meso position,[36] and the boron substituents.[37] They are currently used as chromogenic probes,[38] fluorescent switches,[39] electrochemiluminescent materials,[40,41] laser dyes,[42] fluorescent labels for biomolecules,[37] drug delivery agents,[43] and as electron-transfer probes for radical ion pairs generated by local electric fields.[44] All these fascinating applications attest the exceptional robustness and processability of these nonionic dyes allowing their sublimation under high vacuum to provide electroluminescent layers.[41]

However, frequently encountered deficiencies in the use of Bodipy in photon or electron responsiveness molecular devices are difficulties in organizing these dyes into predictable assemblies such as liquid crystalline materials or supramolecular gels. We recently discovered that amphipathic alkoxydiacylamido platforms bearing chelating oligopyridine cores are able to self-assemble into columnar mesophases and fibrous networks by means of intermolecular hydrogen bonds.[45]

(9) van Bommel, K. J. C.; van der Pol, C.; Muizebelt, I.; Friggeri, A.; Heeres, A.; Meetsma, A.; Feringa, B. L.; van Esh, J. *Angew. Chem. Int. Ed.* **2004**, *43*, 1663.
(10) Würthner, F.; Hanke, B.; Lysetska, M.; Lambright, G.; Harms, G. S. *Org. Lett.* **2005**, *7*, 967.
(11) Tamaru, S.; Nakamura, M.; Takeuchi, M.; Shinkai, S. *Org. Lett.* **2001**, *3*, 3631.
(12) Claussen, R. C.; Rabatic, B. M.; Stupp, S. I. *J. Am. Chem. Soc.* **2003**, *125*, 12680 and references therein.
(13) Menger, F. M.; Peresypkin, A. *J. Am. Chem. Soc.* **2003**, *125*, 5340.
(14) Mukhopadhyay, S.; Maitra, U.; Iar; Krishnamoorthy, G.; Schmidt, J.; Talmon, Y. *J. Am. Chem. Soc.* **2004**, *126*, 15905.
(15) Lopez, F.; Samseth, J.; Mortensen, K.; Rosenqvist, E.; Rouch, J. *Langmuir* **1996**, *12*, 6188.
(16) An, B. K.; Lee, D. S.; Lee, J. S.; Park, Y. S.; Song, H. S.; Park, S. Y. *J. Am. Chem. Soc.* **2004**, *126*, 10232.
(17) Shirakawa, M.; Fujita, N.; Shinkai, S. *J. Am. Chem. Soc.* **2003**, *125*, 9902.
(18) Wang, C.; Zhang, D.; Zhu, D. *J. Am. Chem. Soc.* **2005**, *127*, 16372.
(19) (a) Lee, K. Y.; Mooney, D. J. *Chem. Rev.* **2001**, *101*, 1869. (b) Tiller, J. C. *Angew. Chem. Int. Ed.* **2003**, *42*, 3072.
(20) (a) Aldred, M. P.; Eastwood, A. J.; Kelly, S. M.; Vlachos, P; Contoret, A. E. A.; Farrar, S. R.; Mansoor, B.; O' Neill, M.; Tsoi, W. C. *Chem. Mater.* **2004**, *16*, 4928. (b) Kawamoto, M.; Mochizuki, H.; Ikeda, T.; Lee, B.; Shirota, Y. *J. Appl. Phys.* **2003**, *94*, 6442. (c) Tokuhisa, H; Era, M.; Tsutsui, T. *Appl. Phys. Lett.* **1998**, *72*, 2639. (d) O'Neill, M.; Kelly, S. M. *Adv. Mater.* **2003**, *15*, 1135.
(21) (a) Greeg, B. A.; Fox, M. A.; Bard, A. J. *J. Phys. Chem.* **1990**, *94*, 1586. (b) Fox, A. M.; Grant, J. V.; Melamed, D.; Torimoto, T.; Liu, C.-Y.; Bard, A. J. *Chem. Mater.* **1998**, *10*, 1771. (c) Schmidt-Mende, L.; Fechtenkötter, A.; Müllen, K.; Moons, E.; Friend, R. H.; MacKenzie, J. D. *Science* **2001**, *293*, 1119. (d) Kubo, W.; Kambe, S., Nakade, S.; Kitamura, T.; Hanabusa, K.; Wada, Y.; Yanagida, S. *J. Phys. Chem. B* **2003**, *107*, 4374.
(22) Sagawa, T.; Fukugawa, S.; Yamada, T.; Ihara, H. *Langmuir* **2002**, *18*, 7223.
(23) Engelkamp, H.; Middelbeek, S.; Nolte, R. J. M. *Science* **1999**, *284*, 785.
(24) (a) Jonkheijm, P.; Hoeben, F. J. M.; Kleppinger; R.; van Herrikhuyzen, J.; Schenning, A. P. H. J.; Meijer, E. W. *J. Am. Chem. Soc.* **2003**, *125*, 15941. (b) Ajayaghosh, A.; George, S. J. *J. Am. Chem. Soc.* **2001**, *123*, 5148. (c) George, S. J.; Ajayaghosh, A. *Chem. Eur. J.* **2005**, *11*, 3217. (d) Hulvat, J. F.; Sofos, M.; Tajima, K., Stupp, S. I. *J. Am. Chem. Soc.* **2005**, *127*, 366.
(25) (a) Sugiyasu, K.; Fujita, N.; Shinkai, S. *Angew. Chem. Int. Ed.* **2004**, *43*, 1229. (b) Würthner, F.; Hanke, B.; Lysetska, M.; Lambright, G.; Harms, G. S. *Org. Lett.* **2005**, *7*, 967.
(26) Tang, B. Y.; ge, J. J.; Zhang, A.; Calhoun, B.; Chu, P.; Wang, H.; Shen, Z.; Harris, F. W.; Cheng, S. Z. D. *Chem. Mater.* **2001**, *13*, 78.
(27) Seo, S. H.; Chang, J. Y. *Chem. Mater.* **2005**, *17*, 3249.
(28) An, B.-K.; Lee D.-S.; Lee J.-S.; Park, Y.-S.; Song, H.-S.; Park, S. Y. *J. Am. Chem. Soc.* **2004**, *126*, 10232.
(29) Murata, K.; Aoki, M.; Suzuki, T.; Harada, T.; Kawabata, H.; Komori, T.; Ohseto, F.; Ueda, K. Shinkai, S. *J. Am. Chem. Soc.* **1994**, *116*, 6664.
(30) Ryu, S. Y.; Kim, S.; Seo, J.; Kim, Y.-W.; Kwon, O.-H.; Jang, D.-J.; Park, S. Y. *Chem. Commun.* **2004**, 70.
(31) (a) Nakashima, T.; Kimizuka, N. *Adv. Mater.* **2002**, *14*, 1113. (b) Kishimura, A.; Yamashita, T.; Aida, T. *J. Am. Chem. Soc.* **2005**, *127*, 179.
(32) Kollmannsberger, M.; Rurack, K.; Resch-Genger, U.; Daub, J. *J. Phys. Chem. A* **1998**, *102*, 10211.
(33) Burghart, A.; Kim, H.; Wech, M. B.; Thorensen, L. H.; Reibenspies, J.; Burgess, K. *J. Org. Chem.* **1999**, *64*, 7813.
(34) Ulrich, G.; Ziessel, R. *J. Org. Chem.* **2004**, *69*, 2070.
(35) (a) Haugland, R. P.; Kang H. C. *US Patent US* **1998**, *4*, 774, 339. (b) Thoresen, L. H.; Kim, H.; Welch, M. B.; Burghart, A.; Burgess, K. *Synlett* **1998**, 1276.
(36) Goze, C.; Ulrich, G.; Charbonnière, L.; Ziessel, R. *Chem. Eur. J.* **2003**, *9*, 3748.
(37) Ulrich, G.; Goze, C.; Guardigli, M.; Roda, A.; Ziessel, R. *Angew. Chem. Int. Ed.* **2005**, *44*, 3694.
(38) (a) Wagner, R. W.; Lindsey, J. S. *Pure Appl. Chem.* **1996**, *68*, 1373. (b) Beer, G.; Rurack, K.; Daub, J. *Chem. Commun.* **2001**, 1138. (c) Turfan, B., Akkaya, E. U. *Org. Lett.* **2002**, *4*, 2857. (d) Beer, G.; Niederalt, C.; Grimme, S.; Daub, J. *Angew. Chem. Int. Ed.* **2000**, *39*, 3252. (e) Kollmannsberger, M.; Rurack, K., Resch-Genger, U., Rettig, W.; Daub, J. *Chem. Phys. Lett.* **2000**, *329*, 363. (f) Sancenon, F.; Martinez-Manez, R.; Soto, J. *Angew. Chem. Int. Ed.* **2002**, *41*, 1416.
(39) Golovkova, T. A.; Kozlov, D. V.; Neckers, D. C. *J. Org. Chem.* **2005**, *70*, 5545.
(40) Lai, R. Y., Bard, A. J. *J. Phys. Chem. B.* **2003**, *107*, 5036.
(41) (a) Brom J. M., Jr.; Langer, J. L. *J. Alloys Compd.* **2002**, *338*, 112. (b) Hepp, A.; Ulrich, G.; Schmechel, R., von Seggern, H., Ziessel R. *Synth. Met.* **2004**, *146*, 11.
(42) (a) Chen, T., Boyer, J. H., Trudell, M. L. *Heteroat. Chem.* **1997**, *8*, 51. (b) Sathyamoorthi, G., Wolford, L. T., Haag, A. M., Boyer, J. H. *Heteroat. Chem.* **1994**, *5*, 245.
(43) McCusker, C.; Carroll, J. B.; Rotello, V. M. *Chem. Commun.* **2005**, 996.
(44) Debreczeny, M. P.; Svec, W. A.; Wasielewski, M. R. *Science* **1996**, *274*, 584.

Scheme 1[a]

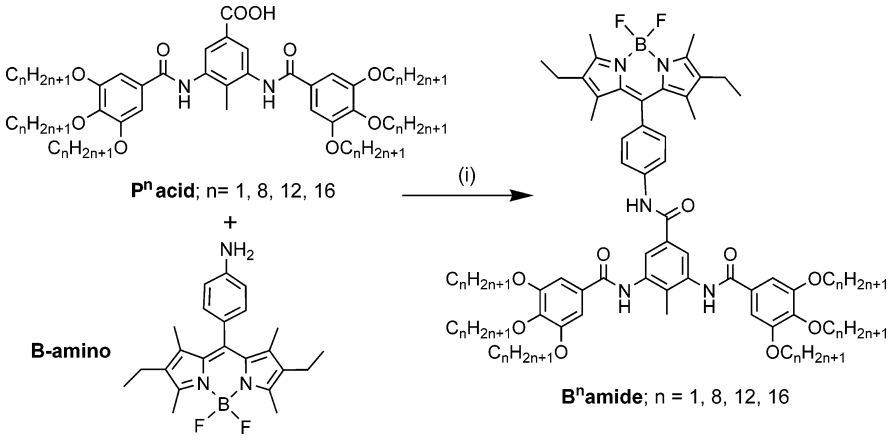

[a] Reagents and conditions: (i) EDC·HCl (2 equiv), DMAP (2 equiv), CH_2Cl_2/THF, rt; $n = 1$, 40%; $n = 8$, 49%; $n = 12$, 48%; $n = 16$, 62%.

Scheme 2[a]

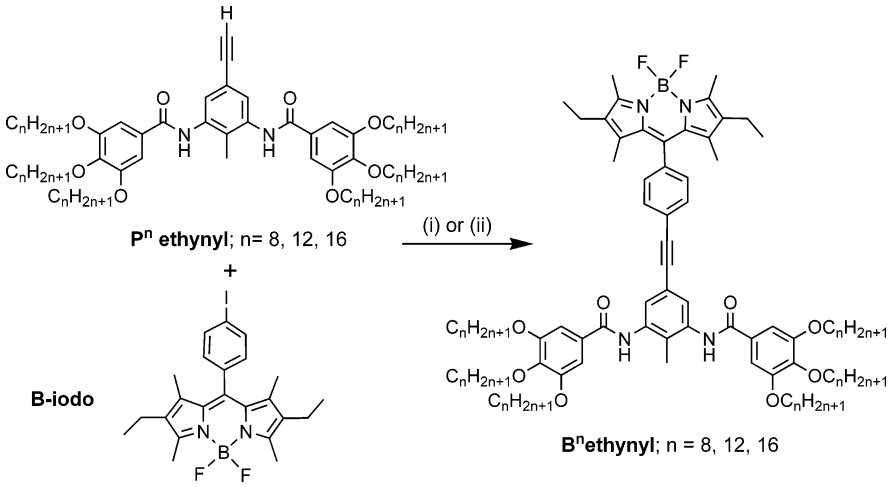

[a] Reagents and conditions: (i) $[Pd(PPh_3)_2Cl_2]$ (6 mol %), $(^iPr)_2NH$, CuI (10 mol %) THF, rt, $n = 12$, 72%, (ii) $[Pd(PPh_3)_4]$ (6 mol %), benzene/triethylamine, 60 °C, $n = 8$, 85%; $n = 16$, 79%.

Therefore, we wish to report herein that a Bodipy framework adequately functionalized with 3,5-diacylamido platforms provides a unique opportunity to study highly luminescent mesomorphic materials and supramolecular gels and that fluorescence spectroscopy could be used to probe the mergent texture of the liquid-crystalline phases and the nature of the aggregates involved in the gels. Preliminary information dealing with some properties of a single compound reported here has already been communicated.[46]

Results and Discussion

Synthesis. The synthesis of the B^{n}amide compounds with six aliphatic chains ($n = 8$, 12, 16) required a cross-coupling reaction between functionalized platforms (in the acid form)[45] and the Bodipy amino derivative[47] in the presence of the hydrochloride salt of 1-ethyl-3-[3-(dimethylamino)propyl]-carbodiimide (EDC·HCl) and dimethylaminopyridine (DMAP) (Scheme 1).

The B^{n}ethynyl molecules were obtained in good yields by a Sonogashira cross-coupling reaction between the platform derivatives bearing an ethynyl function[45a] and an iodo-phenyl-Bodipy[48] in the presence of a catalytic amount of low valent palladium(0) (Scheme 2).[49]

The purification of all materials B^{n}amide and B^{n}ethynyl was achieved by chromatography on silica gel followed by crystallization in a CH_2Cl_2/CH_3CN mixture. Molecular structures and purity were assigned by ^1H, ^{13}C, and ^{11}B NMR, mass spectroscopy, and elemental analysis. In particular, 2D COSY and NOESY NMR experiments performed with the B^{16}amide compound in $CDCl_3$ confirm the existence of intermolecular interactions in relatively concentrated solution ($C = 10^{-2}$ mol·L^{-1}) (Figure 1). In particular, a strong dipolar interaction can be observed between the protons from the

(45) (a) Camerel, F.; Ulrich, G.; Ziessel, R. *Org. Lett.* **2004**, *6*, 4171. (b) Ziessel, R.; Pickaert, G.; Camerel, F.; Donnio, B.; Guillon, D.; Cesario, M.; Prange, T. *J. Am. Chem. Soc.* **2004**, *126*, 12403.
(46) Camerel, F.; Bonardi, L.; Schmutz, M.; Ziessel, R. *J. Am. Chem. Soc.* **2006**, *128*, 4548.
(47) Azov, V. A.; Skinner, P. J.; Yamakoshi, Y.; Seiler, P.; Gramlich, V.; Diederich, F. *HeIv. Chim. Acta* **2003**, *86*, 3648.
(48) Burghart, A.; Kim, H.; Welch, M. B.; Thoresen, L. H.; Reibenspies, J.; Burgess, K.; Bergstroem, F.; Johansson, L. B.-A. *J. Org. Chem.* **1999**, *64*, 7813.
(49) Sonogashira, K. In *Comprehensive Organic Synthesis*; Trost, B. M., Fleming, L., Paquette, L. A., Eds.; Pergamon Press: Oxford, 1990; Vol. 3, pp 545−547.

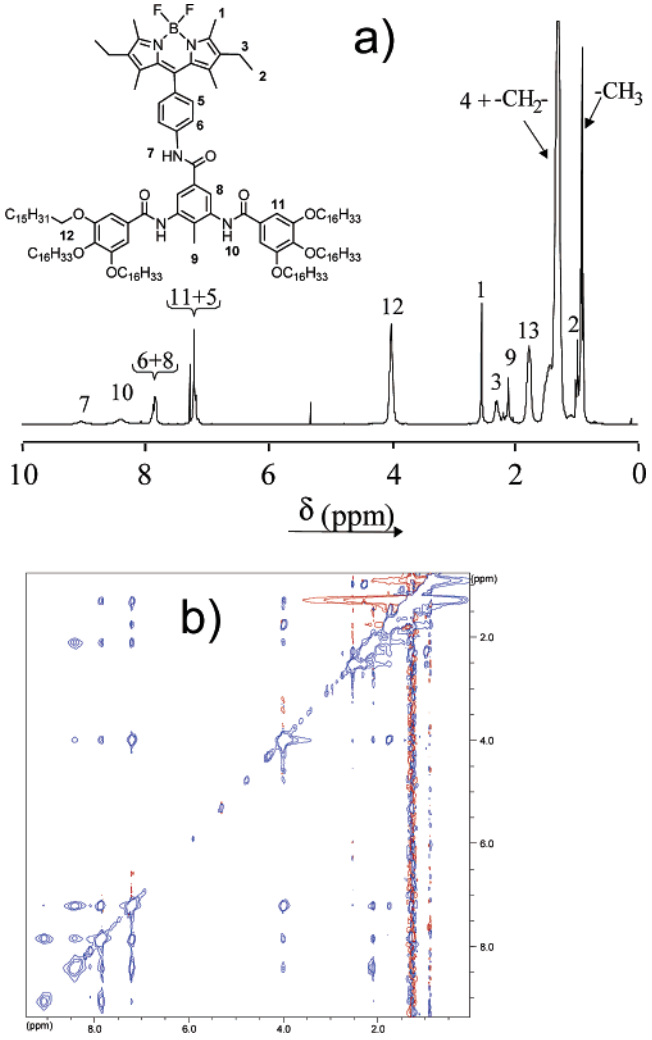

Figure 1. (a) ^{1}H NMR spectrum of B^{16}amide compound in $CDCl_3$ (400 MHz) at 298 K ($C = 10^{-2}$ mol·L^{-1}). (insert) Hydrogen atom numbering scheme. (b) 2D NOESY spectrum.

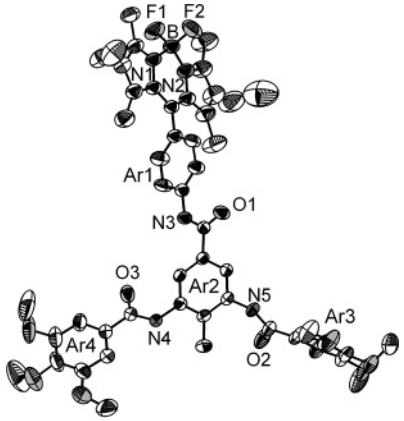

Figure 2. ORTEP drawing of the B^{1}amide compound with the main numbering scheme. Thermal ellipsoids drawn at the 50% probability level.

methyl group on Ar2 and the aromatic hydrogen atoms of Ar2 (see Figure 2 for labeling). This interaction cannot be explained on the basis of the X-ray crystal structure of the B^{1}amide compound since a long intramolecular distance of 4.9 Å can be measured between the hydrogen atoms of the methyl group on the Ar2 phenyl group and its aromatic hydrogen atoms. But, this interaction can be explained by the formation of hydrogen-bonded dimers, as observed in the crystal structure, with a decrease of the intermolecular distance down to 3.9 Å. These results confirm that the hydrogen-bonded dimer motif observed in the crystal structure is robust and can be detected in relatively concentrated solution. Numerous other correlations of possible intermolecular origin can be observed on the spectra, but their unambiguous assignment is hampered by the fortuitous isochronism of the hydrogen atoms of Ar1 phenyl group with hydrogen atoms of Ar2, Ar3, and Ar4 phenyl rings.

Table 1. Spectroscopic Data for the Compounds in Dichloromethane at 298 K

compound	λ_{abs} (nm)	ϵ (M^{-1}·cm^{-1})	λ_F (nm)	Φ_F [a]	τ_F (ns)	k_{RAD} (10^8 s^{-1})	k_{NR} (10^7 s^{-1})
B^{1}amide	525	72 000	540	0.58	7.7	0.75	5.4
B^{8}amide	525	73 000	538	0.62	8.9	0.7	4.2
B^{12}amide	525	70 000	540	0.42	7.5	0.56	7.7
B^{16}amide	525	62 000	538	0.50	7.3	0.68	6.8
B^{8}ethynyl	526	71 500	543	0.51	5.8	0.87	8.4
B^{12}ethynyl	526	73 000	543	0.44	6.4	0.86	7.0
B^{16}ethynyl	526	71 600	543	0.47	6.4	0.73	8.3

[a] Using Rhodamine 6G as reference, $\Phi = 0.78$ in water, $\lambda_{exc} = 488$ nm. All Φ_F are corrected for changes in refractive index.

The optical properties in solution of these functionalized dyes are in good agreement with previously described Bodipy based on 3-ethyl-2,4-dimethyl-pyrrole.[34,36] Spectroscopic data relevant to the present discussion are collected in Table 1. In solution, the absorption spectra of compound B^{n}amide and B^{n}ethynyl show a strong $S_0 \rightarrow S_1$ ($\pi-\pi^*$) transition, centered at 527 nm with absorption coefficients around 70 000 M^{-1}·cm^{-1}, due to the Bodipy chromophore. The much weaker and relatively broad absorption band located around 357 nm is likely assigned to the $S_0 \rightarrow S_2$ ($\pi-\pi^*$) transition located on the Bodipy fragment.[36] The fluorescence behavior was observed at ambient conditions in very dilute dichloromethane solutions. Emission from the Bodipy unit is observed for all compounds, and its profile shows good mirror symmetry with the corresponding absorption band, with a Stokes shift of about 600 cm^{-1}. The measured relative fluorescence quantum yields (Φ_F) are lower (ca. 50%) than for analogous Bodipy derivatives due to the presence of amide groups in the neighborhood of the dye, leading to some nonradiative deexcitation.[37] Emission from the Bodipy unit decays via a first-order kinetics with a lifetime (τ_S) in the 5 to 9 ns range.

Molecular Structure of the B^{1}amide Compound by X-ray Diffraction on a Single Crystal. In order to have a better understanding of the molecular organization of the B^n-amide compounds in the solid state, the homologue B^{1}amide model compound appended with six methoxy groups was synthesized. Indeed, structural information of the molecular arrangements within the crystal phase may be partially preserved in the mesophase and helps in the interpretation of the molecular packing in the liquid crystalline phase.[50] The B^{1}amide compound could be crystallized by slow vapor diffusion of diethylether in a DMSO/H_2O mixture at room temperature. Red plate-like crystals suitable for X-ray analysis were obtained as a pure single phase. The crystal structure was determined by single-crystal X-ray diffraction

(50) Pickaert, G.; Cesario, M.; Ziessel, R. *J. Org. Chem.* **2004**, *69*, 5335−5341.

at 293 K. This compound crystallizes in the triclinic space group $P\bar{1}$ (a = 12.7711(7) Å; b = 13.1721(8) Å; c = 20.3277(10) Å; α = 85.767(3)°; β = 82.301(3)°; γ = 64.957-(2)°, V = 3069.61(30) Å,^{3} Z = 2). The asymmetric unit contains one B^{1}amide molecule and three disordered DMSO molecules in general positions. Figure 2 shows the atomic numbering and labeling scheme of the B^{1}amide compound. As expected, the molecule is nonplanar; the peripheral trisubstituted rings (Ar3 and Ar4) are almost perpendicular with the central phenyl ring (Ar2). The Ar1 phenyl ring is parallel to the central phenyl ring Ar2 (angle Ar1−Ar2 = 23.4°), which in turn orients the Bodipy fragment perpendicular to the central phenyl ring (Ar2) (angle Ar2-Bodipy = 83.7°). One can note that the two amides vectors point in the opposite directions, which is auspicious for the formation of a polymeric hydrogen-bonded network. Different views of the crystal packing in the crystal are presented in Figure 3. The crystal structure is best described as being made of dimers tethered by intermolecular hydrogen bonds. Two molecules are connected, in a centro-symmetric fashion, by two intermolecular hydrogen bonds (N5H----O3 = 2.894-(4) Å and N5HO3 angle = 146.66(19)°). Unfortunately, the formation of an extended one-dimensional network of hydrogen bonds is not observed in this crystal since the dimer engaged its remaining donor−acceptor groups in hydrogen bond with the surrounding DMSO molecules (Figure 3c). But an interesting feature is that the hydrogen-bonded dimers form extended chains running in the [−101] direction through stacking of two Bodipy fragments (mean distance = 5.0 Å) between different dimers (Figure 3b). This dimer is not stabilized by $\pi-\pi$ stacking interactions but by four intermolecular hydrogen bonds between one fluorine atom of the BF_2 fragments on the first molecule and two hydrogen atoms on the phenyl ring Ar1 of the second molecule (C6AH----F1 = 3.279(5) Å; C6AHF1 angle = 110.0°; C5AH----F1 = 3.388(4) Å; C6AHF1 angle = 104.0°).[51] It can be noted that the formation of Bodipy dimers orients the ethyl groups of one fluorophore in the same direction.

Mesomorphic Properties. In a first step, the thermotropic behavior of the B^{n}ethynyl and B^{n}amide molecules was studied by combining thermogravimetric analyses (TGA), differential scanning calorimetry (DSC), polarized optical microscopy with a heating stage (POM), and temperature-dependent wide- and small-angle X-ray diffraction (WAXS, SAXS). From TGA analyses and NMR experiments performed after the DSC measurements, the degradation temperature of the B^{n}ethynyl and B^{n}amide compounds was found to be above 250 °C.

B^{n}ethynyl. The first homologue of the series, B^{8}ethynyl, was deprived of mesomorphism, as deduced by POM, DSC, and X-ray diffraction, melting directly into the isotropic liquid at 237 °C. SAXS and WAXS measurements on powder samples recorded below 237 °C exhibit several sharp peaks in the small-angle region together with a structured broad scattering halo centered at 4.7 Å in the wide-angle region.

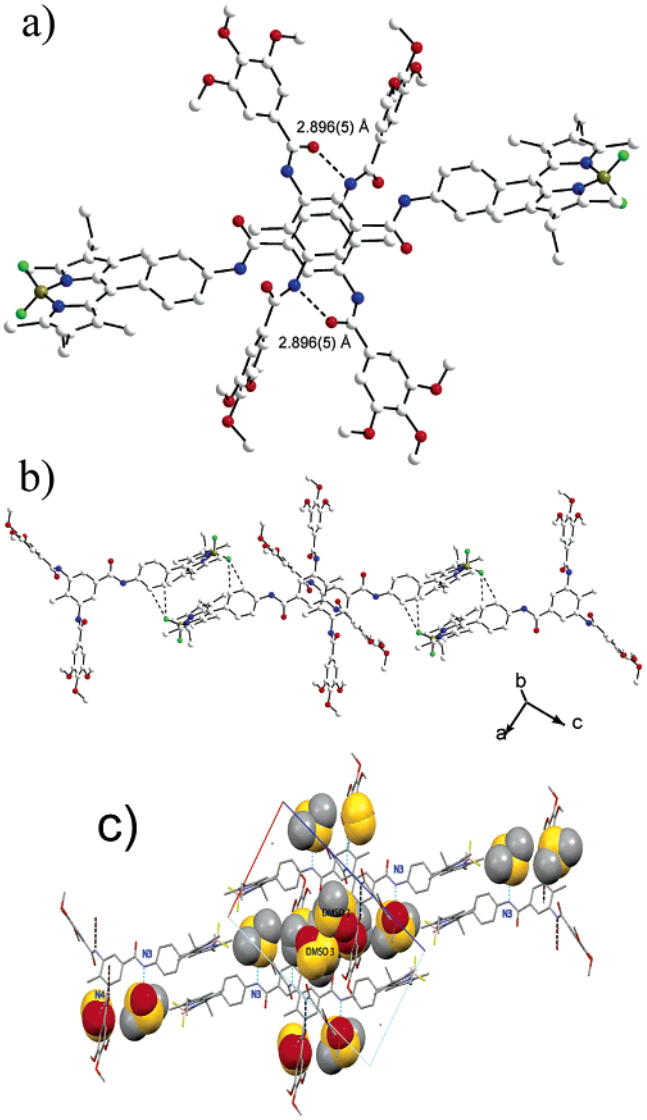

Figure 3. (a) A centro-symmetrical dimer of the B^{1}amide compound. The hydrogen bonds (dotted lines) connect centro-symmetrically the amide groups of two molecules at the (x, y, z) and ($-x$, 1 − y, 1 − z) positions (N5H---O3 = 2.894(4) Å, N5HO3 angle = 146.66(19)°). (b) Chains form in the [−101] direction between hydrogen-bonded dimers via stacking of the Bodipy fragments through HF bonds (dotted lines). (c) Molecular packing view showing the co-crystallized DMSO molecules engaged with the remaining H-bond donor groups along [−101] chains.

More appealing is the thermal behavior of the other derivatives bearing chains with a larger number of carbons. DSC traces of the B^{12}ethynyl compound display three reversible thermal transitions centered at 184 °C, 158 °C, and 74 °C on the first cooling curve (Figure S1 in Supporting Information). Above 184 °C, B^{12}ethynyl compound is in the isotropic fluid state. By POM, on cooling from the isotropic liquid, pseudo-fan-shaped textures with large homeotropic domains, typical of columnar mesophases, develop (vide infra). In the temperature range below 158 °C, the compound becomes more viscous and a clear unidentifiable textural change occurs. XRD patterns obtained in the range of 184−158 °C upon cooling revealed that this compound is liquid crystalline, exhibiting a broad scattering halo centered at ∼4.7 Å in the wide-angle region while one sharp and intense

(51) (a) Howard, J. A. K.; Hoy, V. J.; O'Hagan, D.; Smith, G. T. *Tetrahedron* **1996**, *52*, 12613−12622. (b) Thalladi, V. R.; Weiss, H.-C.; Bläser, D.; Boese, R.; Nangia, A.; Desiraju, G. R. *J. Am. Chem. Soc.* **1998**, *120*, 8702−8710.

Table 2. Thermal Behavior of the Compounds and X-ray Characterization of the Mesophases[a]

compound	onset transition temp/°C (ΔH = enthalpy/kJ·mol^{-1})	d_{meas}/Å	I	hk	d_{calc} /Å	mesophase parameters measured at T	molecular volume at T (V_M)
B[8]ethynyl	PCr 237 (51.17) I						
	I 212 (−41.43) PCr						
B[12]ethynyl	Cr 78 (43.88) PCr 182.5 (26.41)	27.6	VS	10	27.6	T = 183 °C	V_M = 3411 Å^3
	Col$_h$ 187.5 (9.21) I	10.2	br			a = 31.9 Å	
	I 184 (−12.51) Col$_h$ 158 (−25.27)	4.7	br			S = 880 Å^2	
	PCr 74 (−32.07) Cr						
B[16]ethynyl	Cr 64 (8.26) Cr′ 87 (48.92) PCr 141 (22.94) Col$_h$ 171 (11.17) I	30.4	VS	10	30.4	T = 165 °C	V_M = 3988 Å^3
	I 167 (−10.85) Col$_h$ 114 (−18.65) PCr 79 (−38.22) Cr′ 63 (−13.76) Cr	10.7	br	B		a = 35.1 Å	
		4.7	br	A		S = 1067 Å^2	
B[8]amide	Cr 176 (15.20) Col$_h$ dec >250.0	24.7	VS	10	24.7	T = 220 °C	V_M = 2894 Å^3
	>250.0 dec Col$_h$ 123.5 (−11.17) Cr	14.2	M	11	14.2	a = 28.5 Å	
		8.2	br			S = 704 Å^2	
		4.6	br				
B[12]amide	Cr 49 (19.49) PCr 213 (25.49) Col$_h$ 241 (15.52) I	28.0	VS	10	28.0	T = 220 °C	V_M = 3534 Å^3
	I 237 (−16.71) Col$_h$ 138 (−17.91) PCr 46 (−19.12) Cr	4.6	br			a = 32.3 Å	
						S = 904 Å^2	
B[16]amide	PCr 32 (80.23) PCr′ 149 (7.13) Col$_h$ 219 (13.92) I	30.3	VS	10	30.4	T = 200 °C	V_M = 4116 Å^3
	I 214 (−11.86) Col$_h$ 25 (−113.32) PCr	17.65	W	11	17.6	a = 35.1 Å	
		9.4	br	B		S = 1070 Å^2	
		4.6	br	A			

[a] d_{meas} and d_{calc} are the measured and calculated diffraction spacing; I is the intensity of the reflection (VS, very strong; M, medium; W, weak; br, broad); hk are the indexations of the reflections corresponding to the Col$_h$ phase; a is the lattice parameter of the hexagonal columnar phase ($a = 2/(3)^{1/2} \times \langle d_{10} \rangle$ with $\langle d_{10} \rangle = (1/N_{hk})(\sum_{h,k} d_{hk}(h^2 + k^2 + hk)^{1/2}$ where N_{hk} is the number of hk reflections) and S is the lattice area ($S = a \times \langle d_{10} \rangle$); V_M, molecular volume defined by $V_M = (M/0.6022)(V_{CH_2}(T)/V_{CH_2}(T_0))$; M, molecular weight; $V_{CH_2}(T) = 26.5616 + 0.02023T$ (T in °C, T_0 = 25 °C); Cr, crystalline phase; I, isotropic liquid, Col$_h$, hexagonal columnar mesophase; PCr, poorly crystallized material; dec, decomposition temperature.

reflection in the small-angle region is observed. The broad halo corresponds to the average distance between the molten chains attached to the functional platform. Another slightly less diffuse halo can also be observed at 10.2 Å and was attributed to some liquid-like correlations between neighboring molecules. The reflection observed in the small-angle domain is indicative of a repeating unit between large objects. In regard to the texture observed, the molecular shape, and the mesomorphic behavior of structural analogues,[45,52] we were prone to assign the mesophase as a Col$_h$ phase, with a parameter of 31.9 Å at 183 °C. Below 158 °C, XRD patterns display some features on the broad scattering halo, centered at ∼4.7 Å and reveal that the material is poorly crystallized (PCr). Finally, below 74 °C, the XRD patterns display only sharp peaks in the wide-angle region indicative of the formation of a crystalline material.

Four reversible thermal transitions were observed for B[16]-ethynyl compound (DSC) (Table 2 and Figure 4) at 167 °C, 114 °C, 79 °C, and 63 °C on cooling. Above 167 °C, the material is an isotropic liquid. Cooling from the isotropic state, a fluid and pseudo-fan-shaped texture with large homeotropic domains, typical of hexagonal columnar phases, appears under the microscope in the temperature range of 167−114 °C (Figure 5). On further cooling, below 114 °C, the material becomes highly viscous but no textural changes were observed. Below 79 °C, the apparition of cracks on the texture were indicative of a crystalline material. The XRD patterns, obtained in the temperature range of 167−114 °C, displayed a broad scattering halo centered at 4.5 Å (halo A), which proves the fluid-like nature of this phase. In the small-angle region, only one sharp peak was observed as for B[12]ethynyl compound. Based on the optical texture and molecular shape, the mesophase was assigned as Col$_h$ with

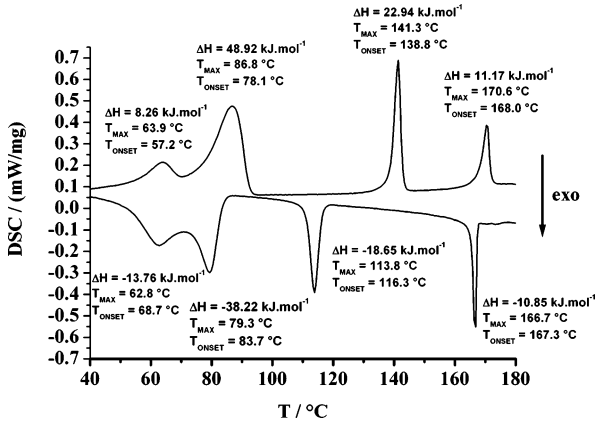

Figure 4. DSC traces of the B[16]ethynyl compound (top: second heating curve; bottom: first cooling curve).

a lattice parameter a = 35.1 Å at 165 °C (Figure S2 in Supporting Information). Another broad halo centered at 10.7 Å was observed and assigned to some liquid-like correlations between neighboring molecules. In the temperature range of 114−79 °C, sharp peaks were observed in the small-angle region together with a structured broad scattering halo centered at 4.7 Å in the wide-angle region, suggesting the formation of a poorly crystalline material. Below 79 °C, a crystalline material is formed. The last transition (63 °C) corresponds to a crystal-to-crystal phase transformation.

As an intermediate statement, it was found that B[8]ethynyl was deprived of mesomorphism over the tested temperature range (mp = 237 °C) whereas the B[12]ethynyl and B[16]ethynyl derivatives exhibited liquid-crystalline phases, assigned as columnar hexagonal mesophases, in the temperature range 184−158 °C and 167−114 °C, respectively (temperatures of the cooling cycle). By increasing the chain length by 4 carbon atoms (24 in total) from octyl to dodecyl, several figures of merit emerged: (i) induction of mesomorphism despite the bulky Bodipy headgroup, (ii) increase of the

(52) Camerel, F.; Ziessel, R.; Donnio, B.; Guillon, D. *New J. Chem.* **2006**, *30*, 135−139.

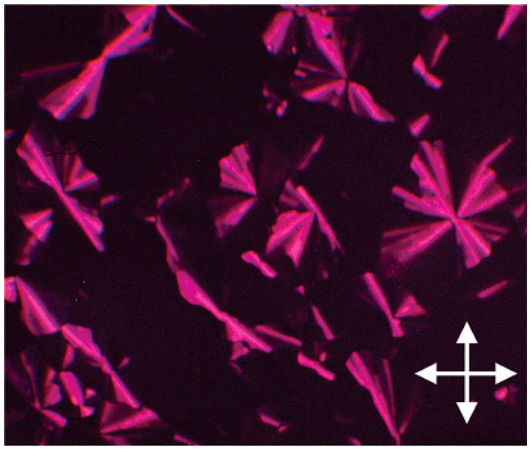

Figure 5. B[16]ethynyl compound viewed by optical microscopy under crossed-polarizers (symbolized by the cross in the corner of the picture) at 162 °C on cooling. The texture exhibits cylindrical domains and large homeotropic regions, pointing to a columnar phase with a hexagonal plane symmetry.

mesomorphic temperature domain from 25 °C for the dodecyl to 51 °C for the hexadecyl derivative, and (iii) decrease of the liquid crystal/crystal transition temperature down to 114 °C for the hexadecyl derivative.

B^{n}amide. The DSC traces of B[8]amide compound display only one reversible thermal transition at 176 °C (on heating). X-ray diffraction patterns recorded below 176 °C displayed several sharp peaks in the whole 2θ ($1° \leq 2\theta \leq 30°$) angular range, in agreement with a crystalline material. Above the transition at 176 °C, the B[8]amide compound appears fluid and birefringent; the clearing point of this compound cannot be determined since degradation occurs over 250 °C. The XRD pattern measured at 220 °C displays two peaks in the small angle region in a ratio of $1:\sqrt{3}$, which can be unambiguously indexed as the (10) and (11) reflections of an hexagonal lattice with a lattice parameter $a = 28.5$ Å. In the WAXS region, a broad halo centered at 4.6 Å is observed which confirms the fluid-like nature of the material at this temperature. Another broad halo is also observed at 8.2 Å and is attributed to some correlations between neighboring molecules (mean distance between the core of the molecules).

B[12]amide compound displays three reversible transitions at 237 °C, 138 °C, and 46 °C on the first DSC cooling curve (Figure S3 in Supporting Information). Above 237 °C, the material is isotropic. On cooling, a pseudo-fan-shaped texture, typical of hexagonal columnar phase, develops. XRD patterns, in the small-angle region, display only one sharp peak. This peak indexed as the (10) reflection in an hexagonal lattice, leads to a lattice parameter $a = 32.3$ Å at 220 °C. In the wide-angle region, a broad halo centered at 4.7 Å was observed and confirms the fluid-like nature of the material. Below 138 °C, the broad halo becomes more structured (PCr), and then below 46 °C, a crystalline state can be clearly identified with the appearance of several sharp peaks in the small- and wide-angle regions.

Finally, B[16]amide is mesomorphic between 214 and 25 °C (Figure S4 in Supporting Information). At 230 °C, the material is fluid and isotropic. In the temperature range of 214−25 °C, typical textures of a hexagonal columnar mesophase can be observed with pseudo-fan-shapes surrounded by large homeotropic domains. XRD patterns obtained at 200 °C display, in the small-angle region, two sharp peaks in the ratio $1:\sqrt{3}$, which can be unambiguously indexed in a hexagonal lattice with a lattice parameter $a = 35.1$ Å (Figure 6). In the wide-angle region, a broad scattering halo centered at 4.6 Å (halo A) is observed and proves the fluid-like nature of this phase. Another broad halo is also observed at 9.4 Å and was attributed to some correlations between neighboring molecules (mean distance between the cores of the molecules). XRD patterns below 25 °C after heating did not exhibit any sharp reflections but only a "sharp" halo, indicative of a poorly crystallized material. In the second heating run between the transitions at 32 and 149 °C, another poorly crystallized material is observed that changes to a liquid-crystalline hexagonal columnar phase between 149 °C and 219 °C.

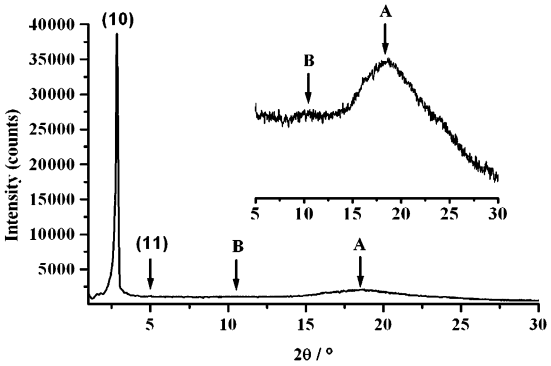

Figure 6. XRD pattern of the B[16]amide compound at 200 °C on cooling.

As would be expected by the presence of a third amide structuring function, all B^{n}amide compounds ($n = 8$, 12, 16) are mesomorphic over a large temperature range with the existence of hexagonal columnar mesophases. It appears that the substitution of the ethynyl link by an additional binding amide function enhances the hexagonal columnar mesophase stability, as shown in particular by an increase of the clearing point. All the results of this investigation are gathered in Table 2.

FT-IR Spectroscopy in the Mesophases. The role of intermolecular hydrogen bonding in the mesophase architecture was probed by variable-temperature FT-IR spectroscopy for B[16]ethynyl and B[16]amide samples dispersed into anhydrous KBr pellets. For B[16]ethynyl compound, a weakening of the ν_{NH} stretching vibrations with a shift from 3175 cm^{-1} in the crystalline phase to 3312 cm^{-1} in the isotropic phase was observed. In the crystalline phases, in the semicrystalline phase and in the mesophase, the C═O stretching vibration appears and remains as a single band at 1639 cm^{-1}. In the isotropic phase (above 170 °C), this band is enlarged and shifts to 1665 cm^{-1}. The shift observed during the mesophase-to-isotropic liquid-phase transition indicates that a large part of the hydrogen-bonded network is disrupted and that weaker hydrogen-bonded amide groups are likely formed. Upon cooling, below the high-temperature transition at 167 °C, the hydrogen-bonded network is reconstructed, the C═O stretching vibration reappears as a single sharp band at 1639 cm^{-1}, and the ν_{NH} stretching vibration shifts from 3312 cm^{-1} to 3175 cm^{-1}. The presence of a single C═O stretching band in the mesophase indicates that all the amide

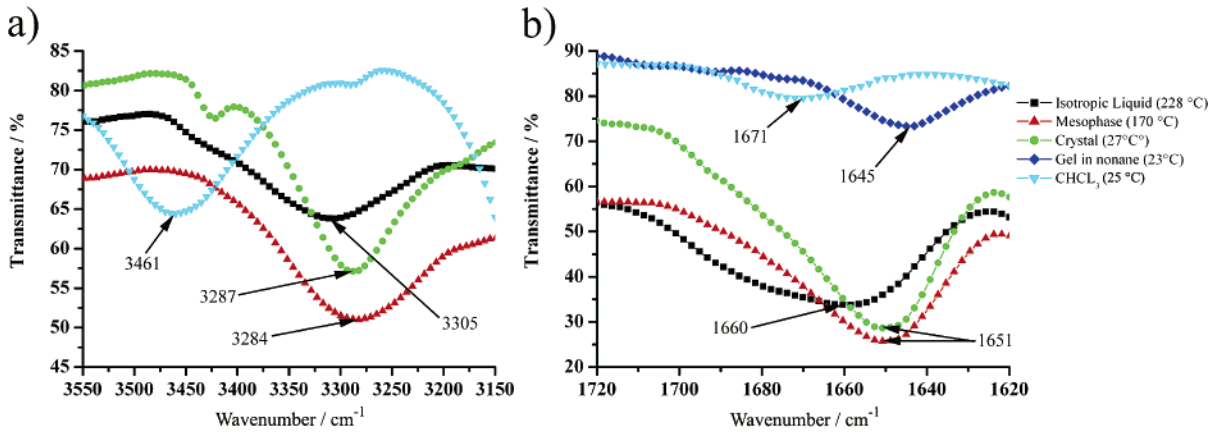

Figure 7. FT-IR for B[16]amide in various states of matter and in $CHCl_3$ solution: (a) ν_{NH} stretching vibration and (b) ν_{CO} stretching vibration. Gel in nonane (C = 14.1 mmol·L^{-1}).

groups on the B[16]ethynyl molecules are involved in hydrogen bonding. These latter values are in agreement with previous studies performed on mesogenic hydrogen-bonded amide aggregates.[53]

In the case of B[16]amide compound (Figure 7), a broad ν_{NH} band centered at 3305 cm^{-1} and a large ν_{CO} band centered at 1660 cm^{-1} were found at 228 °C in the isotropic state. These values are indicative of a distribution of amide functions involved in hydrogen bonds of different strengths. At 170 °C, in the Col_h phase, a strong ν_{NH} band at 3284 cm^{-1} and a sharp ν_{CO} band at 1651 cm^{-1} were found, consistent with strong hydrogen bonding through the amide groups. The absence of non-hydrogen-bonded amides suggests a well-organized state of matter.[45b] At 27 °C in the semi-crystalline phase, no additional changes were observed on the IR spectra. Dissolving the B[16]ethynyl and B[16]amide compounds in $CHCl_3$ or CH_2Cl_2 (ca. 10^{-3} M), hydrogen bonding is likely to be less effective, as confirmed by the ν_{NH} at 3461 cm^{-1} and ν_{CO} at 1671 cm^{-1} frequencies in $CHCl_3$ and by the ν_{NH} at 3417 cm^{-1} and ν_{CO} at 1677 cm^{-1} frequencies in CH_2Cl_2. These values are characteristic of free amide functions.[54]

Temperature Dependence of the Luminescence in the Solid State and Mesophase. Observed upon UV irradiation at 356 nm or with a fluorescence microscope (300 < λ_{ex} < 350 nm), all the compounds appear highly luminescent in the solid state (Figure S5 in the Supporting Information). In order to probe the emission properties of the Bodipy fluorophore in the various material states detected by DSC and XRD, temperature-dependent fluorescence experiments were performed on the B[16]ethynyl compound with the help of a fluorescence microscope equipped with a heating stage. At temperatures above 167 °C, in the isotropic state, all the molecules are randomly distributed. The luminescence appears yellow-green and completely uniform inside the fluid material. It is interesting to note that the luminescence remains very strong even at high temperatures. Cooling below 167 °C, in the liquid-crystalline state, the typical texture of the hexagonal phase with pseudo-fan-shaped texture and large homeotropic domains is observed by POM (Figure 8a). Now, the luminescence observed upon irradiation at 300 < λ_{ex} < 350 nm without any polarizer is not uniform, and domains with different real color emission can be observed (Figure 8b). The emission of the different bright and dark domains likely matches the texture observed in transmission between crossed-polarizers (Figure 8c). From this superimposition of the classical texture and the texture obtained by luminescence, it appears that the emission seems to be correlated to the different molecule orientations inside the mesophase. In the semi-crystalline phase between 114 and 179 °C, no real change is observed on both classical and fluorescence textures. However, a global color change is observed in emission from yellow-green to orange-yellow during the transition, attributed to the formation of excited oligomers resulting in a bathochromic shift of the emitted light. Below 79 °C, cracks appeared in the texture observed by transmission between crossed-polarizers. These cracks give strong red luminescence, tentatively attributed to the decrease of the layer thickness (a prototypic example is given for B[16]ethynyl in Figure S6 in Supporting Information). Bright pseudo-fan-shapes reminiscent of the mesophase are clearly observed by fluorescence microscopy and confirm that the colors of the emitted light are correlated to the column extension and orientation. To our knowledge, this is the first time that the texture of a thermotropic liquid-crystal is observed by fluorescence microscopy.

Packing Modeling of B[16]amide Compound inside the Mesophase. As mentioned in the introduction, there exist several elegant methods to enhance the attractive interactions between disk-like mesogens in order to form stable columns. One commonly used approach consists in the incorporation within the molecule of several hydrogen-bonding sites (e.g., amide groups)[55] or to consider aza-macrocycles, such as hexaazatriphenylene.[56] In an alternative approach, hydrogen-bonding motifs may also run along the inner column core.[57] Such motifs included within the molecular frame will play an important role in the way the molecules stack and are considered in the description of the columnar packing.

In the approach described here, the pseudo-disk-like molecule bears three amide functions along a Bodipy moiety.

(53) (a) Kato, T.; Kutsuna, T.; Hanabusa, K.; Ukon, M. *Adv. Mater.* **1998**, *10*, 606. (b) Silverstein, R. M.; Bassler, G. C.; Morrill, T. C. *Spectrometric Identification of Organic Compounds*, 3rd ed.; Wiley: New York, 1976. (c) Hanabusa, K.; Kato, C.; Kimura, M.; Shirai, H.; Kakehi, A. *Chem. Lett.* **1997**, 429.

(54) Suzuki, M.; Yumoto, M.; Kimura, M.; Shirai, H.; Hanabusa, K. *Tetrahedron Lett.* **2004**, *45*, 2947.

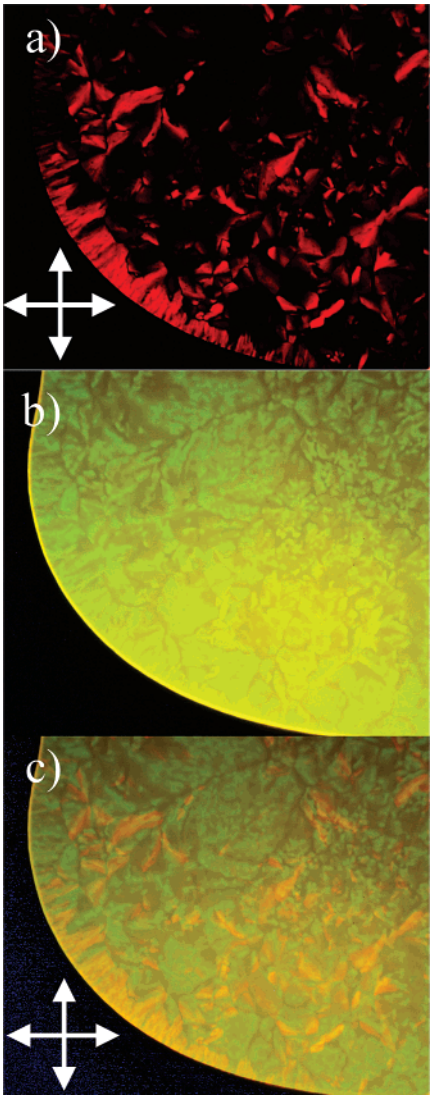

Figure 8. Drop of B[16]ethynyl compound observed by optical microscopy at 162 °C : (a) with a white light in transmission between crossed-polarizers (symbolized by the cross in the corner of the picture) (classical texture); (b) upon irradiation at $300 < \lambda_{ex} < 350$ nm (emission texture without any polarizer); (c) Overlapping of panels a and b.

From the crystalline structure of the methoxy B[1]amide derivative, it was clearly observed that primary hydrogen-bonded dimers (the platform) were formed, with the latter being connected to each other to generate extended chains through the stacking of two neighboring Bodipy fragments. Additionaly, intermolecular hydrogen bonds involving the BF_2 moieties are also effective. The molecular packing within the columnar phase may partially retain some of these structural features. Furthermore, temperature-dependent FT-IR measurements and 2D NMR experiments have revealed that the hydrogen-bonded dimer is robust. This motif was used as an elementary building block for the molecular modelization. In the model proposed, the staggered dimer behaves nearly as classical flat and rigid disk, stacking on top of each other to form columns. The columns may be further stabilized by intra-columnar interactions through the Bodipy fragments between dimers, despite the presence of the long aliphatic chains which will reduce the tendency for such interactions. Molecular dynamics was used in order to justify the model and to correlate the fundamental distances with the molecular dimension.

A periodic molecular model for B[16]amide compound was built from the experimental X-ray data, that is, a hexagonal cell with a lattice parameter $a = 35.1$ Å and a thickness of 15.2 Å, corresponding to four stacked molecules (4×3.8 Å) (Figure 9a,b). This value of 3.8 Å corresponds to the average stacking periodicity and was extracted from the SAXS measurements ($h = V_M/S$). The result of the calculation evidenced a good filling of the available volume, acknowledged by a calculated density of 0.95 (Figure 9c). An enhancement of the micro-segregation over the entire simulation experiment time was also observed, the aliphatic chains totally embedding the inner core as well as the Bodipy fragments, contributing to the stabilization of the edifice.

Furthermore, it was found that the stacking of the central molecular cores stabilized by H-bonding was retained from the crystalline structure (average distance ca. 3.8 Å), with a regular alternation of the side Bodipy groups. Additionally, hydrogen interactions between Bodipy species through the BF_2 fragment within the column were also observed, with a mean distance of nearly 3.8 Å. The Bodipy-containing part does not lie in the same plane as the central molecular core but is tilted with respect to the lattice plane allowing for a closer contact (Figure 9b). Of course, this is only a simplified view of the local arrangement at the molecular level, this stacking likely not extend over too great a distance due to the absence of characteristic peaks within the XRD pattern.

Gelation Properties of the B[16]amide Compound. It was found recently that such functionalized platforms bearing amide functions are able to gel organic solvents through the aggregation of the molecules into elongated fibers induced by an extended network of hydrogen bonds.[45,58,59] For these reasons, the gelation ability of the B[n]amide compounds bearing three amide functions was evaluated in various polar or unpolar, protic or non-protic solvents (see Table S3 in Supporting Information). Only the B[16]amide compound displayed excellent gelation abilities in linear alkanes from C_9 to C_{12} carbon chains and in dimethylformamide (Figure 10a). Stable and robust gels were formed at 25 °C after the mixture of the compound and the organic solvent were heated to form a homogeneous fluid solution. When observed upon

(55) (a) Matsunaga, Y.; Miyajima, N.; Nakayasu, Y.; Sakai, S.; Yonenaga, M. *Bull. Chem. Soc. Jpn.* **1988**, *61*, 207−210. (b) Brunsveld, L.; Schenning, A. P. H. J.; Broeren, M. A. C.; Janssen, H. M.; Vekemans, J. A. J. M.; Meijer, E. W. *Chem. Lett.* **2000**, *29*, 292−293. (c) van Gestel, J.; Palmans, A. R. A.; Titulaer, B.; Vekemans, J. A. J. M.; Meijer, E. W. *J. Am. Chem. Soc.* **2005**, *127*, 5490−5494. (d) Bushey, M. L.; Hwang, A.; Stephens, P. W.; Nuckolls, C. *J. Am. Chem. Soc.* **2001**, *123*, 8157−8158. (e) Bushey, M. L.; Hwang, A.; Stephens, P. W.; Nuckolls, C. *Angew. Chem. Int. Ed.* **2002**, *41*, 2828.

(56) Gearba, R. I.; Lehmann, M.; Levin, J.; Ivanov, D. A.; Koch, M. H. J.; Barbera, J.; Debije, M. G.; Piris, J.; Geerts, Y. H. *Adv. Mater.* **2003**, *15*, 1614.

(57) Paraschiv, I.; Giesbers, M.; van Lagen, B.; Grozema, F. C.; Abellon, R. D.; Siebbeles, L. D. A.; Marcelis, A. T. M.; Zuilhof, H.; Sudho, E. J. R. *Chem. Mater.* **2006**, *18*, 968.

(58) (a) Van Gorp, J. J.; Vekemans, J. A. J. M.; Meijer, E. W. *J. Am. Chem. Soc.* **2002**, *124*, 14759. (b) Camerel, F.; Faul, C. F. *J. Chem. Commun.* **2003**, 1958.

(59) Kimura, M.; Kobayashi, S.; Kuroda, T.; Hanabusa, K.; Shirai, H. *Adv. Mater.* **2004**, *16*, 335.

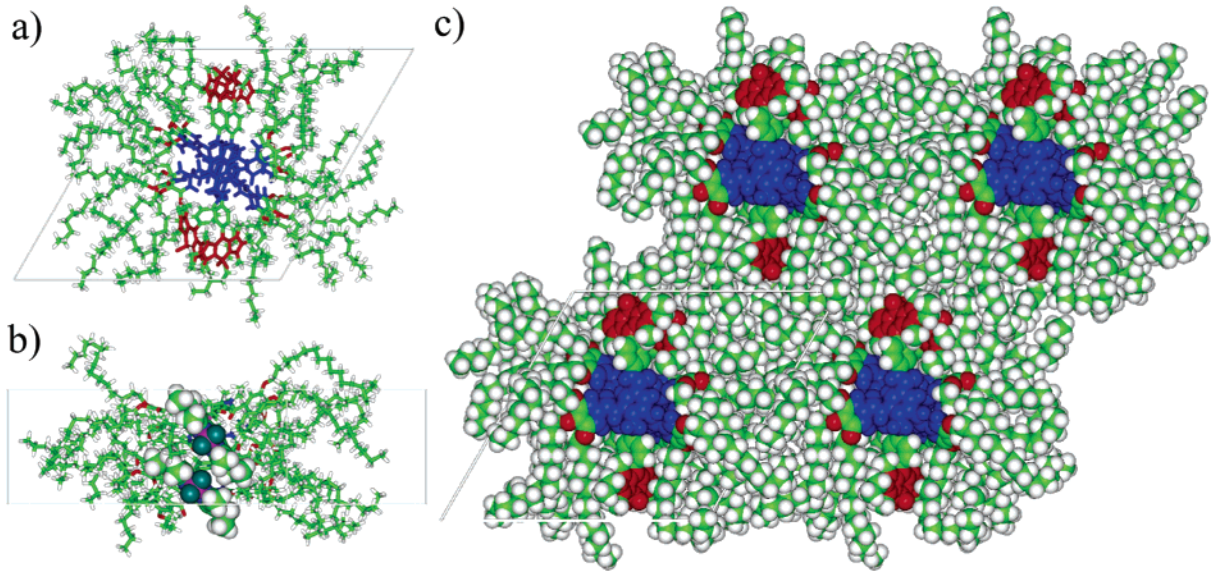

Figure 9. (a) Top view of the packing within a column formed with hydrogen-bonded dimers (polar central core in blue, Bodipy in red). (b) Side view showing the stacking of four B[16]amide molecules (two hydrogen-bonded dimers) and the close Bodipy contacts within the column. (c) Snapshot showing the molecular self-assembling of B[16]amide compounds into the hexagonal lattice of the Col_h phase obtained by a MD calculation.

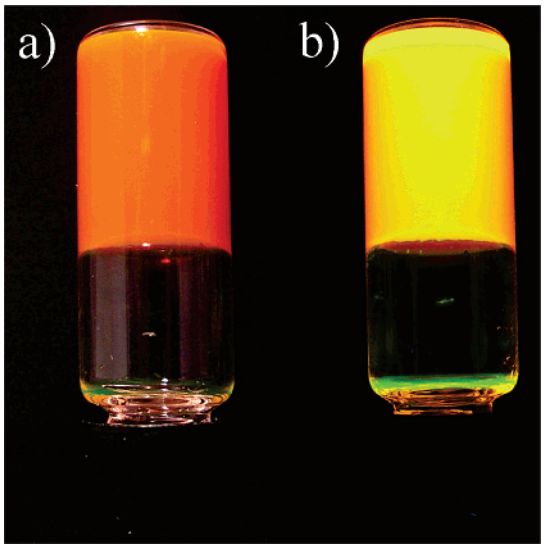

Figure 10. (a) Gelation test of the B[16]amide compound in nonane (10.0 mmol·L^{-1}). (b) Same gel observed upon UV irradiation at 356 nm.

UV irradiation, these gels appear strongly luminescent (Figure 10b). The gel formation criteria used was simply that the solution did not flow when the test tube was turned upside-down at room temperature. The organogels exhibited thermally reversible sol to gel phase transitions. TEM experiments were previously used to examine the morphology of these gel materials and the nature of the aggregated objects that induce the gelation (Figure S7 in Supporting Information).[46]

Temperature Dependence Studies of the Gel. The gelation properties of the B[16]amide compound in nonane were first probed by variable temperature NMR spectroscopy studies. For this purpose, two gels at concentrations of 10.0 mmol·L^{-1} and 14.1 mmol·L^{-1} were prepared. ^{1}H NMR spectra recorded at room temperature of B[16]amide compound in $CDCl_3$ and in nonane displayed distinctly solvent-dependent features. ^{1}H NMR spectrum of B[16]amide compound in $CDCl_3$ showed well-resolved resonance signals in agreement with the molecular structure (see Experimental Section in Supporting Information), whereas in nonane, none of the characteristic signals of the pyrrole core and of the aromatic protons were seen. It should be noted that resonance signals of the B[16]amide below 3 ppm could not be observed owing to overlapping with strong signals of the methylene and the methyl groups of the nonane. These studies confirm that the B[16]amide compound is aggregated in nonane by strong intermolecular interactions and that the resonance signals are completely dampened by motional broadening. As the temperature increases, the resonance signals corresponding to the aromatic protons at 6.77, 6.94, 7.23, 7.51, and 7.61 ppm observed at 85 °C appeared gradually (Figure 11a), along with the -OCH_2 protons at 3.58 and 3.63 ppm (Figure 11b). Upon cooling, the resonance signals observed gradually disappeared and became too broad and weak to be distinguished (increase of the correlation time), confirming that the B[16]amide compound re-aggregates at low temperatures. The same trend can be observed by variable temperature ^{11}B NMR spectroscopy studies (Figure 11c). At room temperature in the gel state, no signal can be detected, but when the temperature increases, a well-defined triplet centered at 3.39 ppm (J_{B-F} = 34.5 Hz), typical of a boron atom coupled with two fluorine atoms, appeared at 75 °C (Figure 11c). This process is reversible, and the signal gradually disappeared upon cooling to room temperature. These observations confirm that the gel formation is induced by the aggregation of the B[16]amide compound into large objects in nonane.

From NMR experiments, the gelation temperature cannot be accurately measured. In order to determine precisely this gelation temperature, DSC experiments and optical microscopy observations under crossed-polarizers were performed on gels. For DSC measurements, the gels were introduced in sealed aluminum pans and scanned in the temperature range of 10−100 °C. DSC traces of the gels at 10.0 mmol·L^{-1} and 14.1 mmol·L^{-1} exhibit one single reversible thermal transition centered at 48.5 °C (ΔH = 0.53 kJ·mol^{-1}) and at 48.1 °C (ΔH = 0.59 kJ·mol^{-1}), respectively, on the

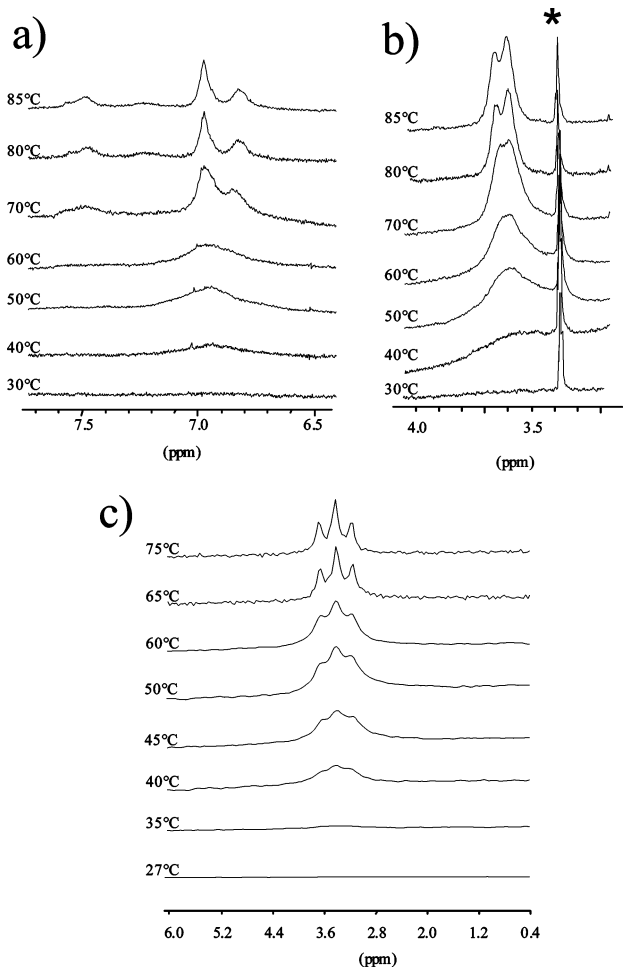

Figure 11. (a) Temperature-dependent ^{1}H NMR spectra of B^{16}amide compound in nonane (10.0 mmol·L^{-1}) for the aromatic protons. (b) Temperature-dependent ^{1}H NMR spectra for the $-OCH_2$ protons. (c) Temperature-dependent ^{11}B NMR spectra. An asterisk (*) corresponds to methanol used as an external reference.

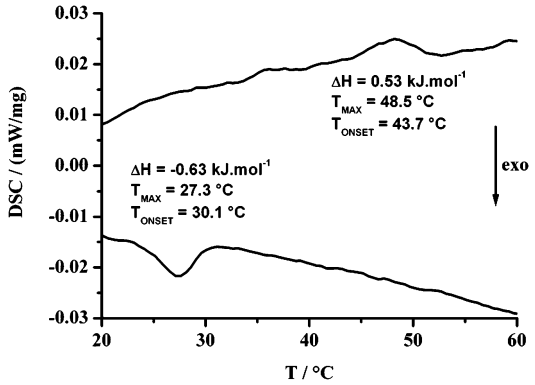

Figure 12. DSC Traces of a gel of the B^{16}amide compound in nonane (10.0 mmol·L^{-1}) (top: second heating curve; bottom: first cooling curve).

heating curves (Figure 12). It should be noted that the nonane has a boiling point of 150.8 °C and a melting point of −51.0 °C.[60] Observations by optical microscopy between crossed-polarizers at room temperature reveal that these materials are viscous and slightly birefringent. These observations are consistent with gel formed by self-assembly of large anisotropic objects. Above the transition temperature at 48.1−48.5 °C, the mixture becomes isotropic (i.e., looks completely dark between crossed-polarizers) and fluid. It appears clearly from the DSC measurements and the POM observations that the phase transition observed at 48.5 °C for the gel at 10.0 mmol·L^{-1} and at 48.1 °C for the gel at 14.1 mmol·L^{-1} on the heating curve is associated with the melting of the gel into an isotropic fluid solution made of smaller aggregates or isolated molecules. Upon cooling, the reverse process is observed at 27.3 °C for the gel at 10.0 mmol·L^{-1} and at 26.9 °C for the gel at 14.1 mmol·L^{-1} with a marked supercooling effect. DSC and POM experiments confirm the existence of a reversible sol−gel thermal transition in the gels.

In order to determine the role played by the amide groups in the thermal gel formation, variable temperature IR spectroscopy studies were performed on the more concentrated gel at 14.1 mmol·L^{-1}. At 23 °C, a single C═O stretching band at 1645 cm^{-1} and a NH stretching band at 3287 cm^{-1} are clear signatures of hydrogen-bonded amides at the origin of hydrogen-bonded network. Upon heating up to 91 °C, no change in the shape, position and intensity of these bands was observed, confirming that the hydrogen-bonded network is not perturbed during the heating process and the melting of the gel. These results confirm that the sol−gel transition observed around 48 °C on heating is not induced by a disruption of the hydrogen-bonded network (i.e., the dismantlement of a supramolecular H-bonded aggregate). Another aggregation process, probably implying the fluorophore parts, is at the origin of the sol−gel transition.

To confirm this hypothesis, variable temperature- and concentration-dependent luminescence measurements were performed on solutions and gels. The absorption spectra of the B^{16}amide compound in dichloromethane and in nonane solutions are presented in Figure 12. In dichloromethane at a concentration of $C = 1.5 \times 10^{-5}$ mol·L^{-1}, the absorption maximum is observed at 525 nm with a pronounced shoulder band at 490 nm. In nonane at a concentration of $C = 3.6 \times 10^{-5}$ mol·L^{-1}, the absorption maximum and the shoulder band are strongly red-shifted to 555 and to 526 nm, respectively (Figure 13a). Upon dilution, an additional absorption band clearly appeared at 526 nm in nonane (Figure 13b). The intensity of the band at 526 nm increases upon dilution while the intensity of the band at 556 nm decreases. The absorption band observed at 525−526 nm in dichloromethane and in nonane can be attributed to the monomeric Bodipy species while the absorption band at 556 nm is due to the absorption of aggregated Bodipy species.

The equilibrium between a monomer (M) and an aggregated species (Agg) containing n monomers is represented by eq 1 and can be developed by the Benesi−Hildebrand treatment[61] according to eqs 2 and 3, where K accounts for the equilibrium constant:

$$n\mathrm{M} \leftrightarrow \mathrm{Agg} \quad (1)$$

$$K = [\mathrm{Agg}]/[\mathrm{M}]^n \quad (2)$$

$$\ln[\mathrm{Agg}] = n \ln[\mathrm{M}] + \text{constant} \quad (3)$$

For each concentration, we have $C_0 = n[\mathrm{Agg}] + [\mathrm{M}]$ where C_0 is the total concentration of B^{16}amide compound in the

(60) *Handbook of Chemistry and Physics*, 54th ed.; CRC Press: Boca Raton, FL, 1973−1974; p C-394.

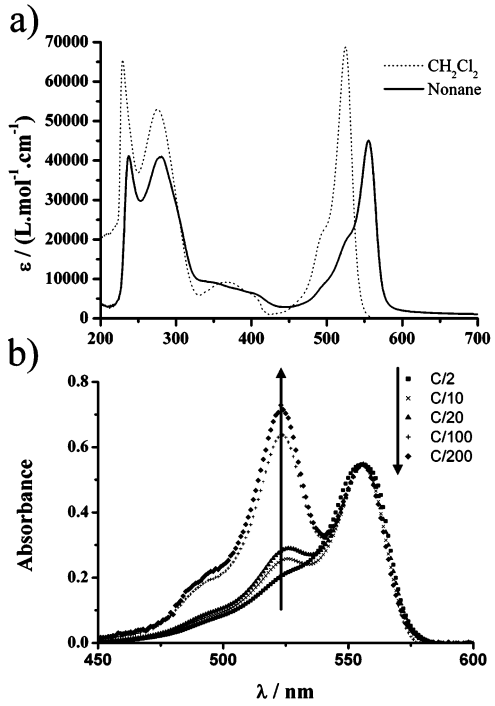

Figure 13. (a) Absorption spectra of B[16]amide in dichloromethane ($C = 1.5 \times 10^{-5}$ mol·L^{-1}) and in nonane ($C = 3.6 \times 10^{-5}$ mol·L^{-1}). (b) Normalized absorption spectra at 555 nm of B[16]amide compound in nonane at different concentrations ($C = 10^{-3}$ mol·L^{-1}).

solution. Since the aggregation number n is assumed to be constant, eq 3 can be written as:

$$\ln(C_0 - (A_M/(\epsilon_M \times l))) = n \ln(A_M/(\epsilon_M \times l)) + \text{constant}' \quad (4)$$

where A_M is the absorbance of the monomer at the concentration C_0, ϵ_M is the molar extinction coefficient of the monomer in nonane, and l is the thickness of the UV cell (0.1 cm).

The molar extinction coefficient of the pure monomer in nonane could not be measured accurately, since the minimum concentration for aggregation was determined to be around 6×10^{-9} mol·L^{-1}.[62] But, with the approximation that the molar extinction coefficient (ϵ_M) in nonane is similar to the one measured in dichloromethane (62000 L·mol^{-1}·cm^{-1}) for the monomeric species and the data extracted from Figure 13b, an aggregation number of 2.1 ± 0.3 can be extrapolated from eq 4 (Figure S8 in Supporting Information).[62] This result indicates that the B[16]amide compound has a strong tendency to form Bodipy dimers in nonane.

The emission spectra of B[16]amide compound in solution and in gel state are presented in Figure 14. In dichloromethane, B[16]amide showed a single intense emission in diluted solution with a maximum at 540 nm and a very weak emission shoulder band at 580 nm upon excitation at 490 nm in the concentration range 10^{-5}–10^{-7} mol·L^{-1} (Table 1 and Figure 14a). Excitation spectrum overlaps the absorption spectrum and confirms that the intense emission at 540 nm

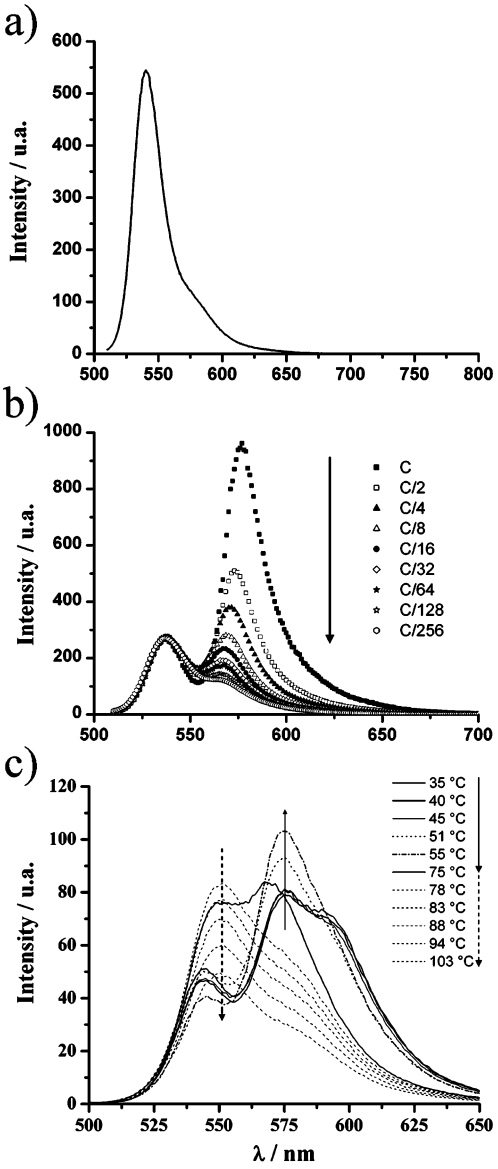

Figure 14. (a) Emission spectrum of B[16]amide compound in CH_2Cl_2 ($C = 9.6 \times 10^{-7}$ mol·L^{-1}) ($\lambda_{ex} = 490$ nm). (b) Normalized emission spectra at 537 nm of B[16]amide in nonane at different concentrations ($C = 3.6 \times 10^{-5}$ mol·L^{-1}) ($\lambda_{ex} = 490$ nm). (c) temperature-dependent emission spectra of a gel from B[16]amide at 10.0 mmol·L^{-1} in nonane ($\lambda_{ex} = 490$ nm).

is due to the emission of isolated Bodipy fragments. However, the emission spectra of the B[16]amide compound in nonane ($c = 3.6 \times 10^{-5}$ mol·L^{-1}) displayed two strong emission bands at 537 and 576 nm upon excitation at 490 nm (Figure 14b). The emission band at 537 nm can be attributed, with respect to the measurements performed in dichloromethane, to the emission of the monomeric Bodipy species, whereas the new red-shifted emission band at 576 nm is likely assigned to the formation of an aggregated Bodipy species (excited dimer). This red-shift of the emission maxima is induced by the formation of molecular *J*-aggregates with a head-to-tail arrangement in which the excitonic energy is delocalized as a result of intermolecular coupling between molecules.[63] A co-facial arrangement as

(61) Benesi, H.; Hildebrand, J. H. *J. Am. Chem. Soc.* **1949**, *71*, 2703.
(62) This approximation is sound by the fact that little variation of the extinction coefficient (± 10%) is found for a model compound [difluororo-8-(*p*-toluyl)-1,3,5,7-tetramethyl-2,6-diethyl-4-bora-3a,4a-diaza-*s*-indacene] in dichloromethane compared to a mixture of nonane (90%) and dichloromethane (10%).
(63) (a) Chen, H.; Farahat, M. S.; Law, K. Y.; Whitten, D. G. *J. Am. Chem. Soc.* **1996**, *118*, 2584. (b) Von Berlepsch, H.; Boettcher, H. C.; Ouart, A.; Burger, C.; Daehne, S.; Kirtsen, S. *J. Phys. Chem. B* **2000**, *104*, 5255.

found in *H*-aggregates would result in a blue shift and is less favorable on steric grounds as deduced from CPK molecular models.[64] As the concentration decreased, the relative emission at 576 nm decreased in favor of the emission at 537 nm, which is in favor of the dismantlement of the excited dimers into the monomeric Bodipy species. These results show that the B^{16}amide compound has a strong tendency to form *J*-mode excited dimer in nonane even at low concentration ($C \sim 10^{-6}$ mol·L^{-1}).

The emission spectrum obtained with the gel at 10.0 mmol·L^{-1} and 35 °C displayed an additional emission band at 592 nm. Upon heating, the emission signal remains constant below the sol−gel transition at 48.5 °C with three emission bands at 544, 575, and 592 nm (Figure 14c). Above the sol−gel transition temperature in the fluid phase the emission at 592 nm disappeared and the emission at 575 nm increases. It appeared that the emission at 592 nm is a signature for the gel formation. Another interesting feature is that a second transition can be observed on the spectra at higher temperature. In fact, between 55 and 78 °C, the emission at 575 nm is transferred to 544 nm. As stated above, the emission at 575 nm can be attributed to the emission of excited dimers and the emission at 544 nm to the emission of the monomeric species. Between 51 and 78 °C upon heating, a breaking up of the excited dimers takes place to form the monomeric species. It should be noted that this second transition at high temperature could not have been observed with all the previous temperature-dependent methods used. Further increase of the temperature leads to the decrease of the luminescence of the monomeric species at 544 nm. The two transitions observed are completely reversible. Upon cooling, the emission at 544 nm first re-increases, then the excited dimers are re-formed, the emission at 544 nm is transferred at 575 nm, and finally, after the gel formation below 27.3 °C, the characteristic emission band of the gel formation at 592 nm re-appeared. This emission band at 592 nm in the gel state can be attributed to the emission of larger fluorophore aggregates ($n > 2$).

A gelification model of nonane by the B^{16}amide compound can now be drawn. As demonstrated by FTIR measurements, the amide fragments of B^{16}amide molecules are always engaged into hydrogen bonds that are not disrupted upon heating. B^{16}amide molecules formed a supramolecular hydrogen-bonded aggregate (at least strong hydrogen-bonded dimers as observed in the X-ray crystal structure and by 2D NMR in relatively concentrated $CHCl_3$ solution). Upon cooling these *J*-bonded supramolecular assemblies first dimerized through the fluorophore part, and then at lower temperature the architecture is densified (i.e., fibril formation), leading to the immobilization of the solvent. The gel formation is a hierarchical process requiring a combination of hydrophobic segregation, hydrogen bonds, and fluorophores interactions in which the fluorophores aggregation is the main driving force for the gel formation.

(64) (a) Tristani-Kendra, M.; Eckhardt, C. J. *J. Chem. Phys.* **1984**, *81*, 1160. (b) Berstein, J.; Goldstein, E. *Mol. Cryst. Liq. Cryst.* **1988**, *164*, 213.

Conclusions

Our results show that grafting of a phenyl substituted 4,4-difluoro-4-bora-3a,4a-diaza-*s*-indacene with 4-methyl-3,5-[bis-3,4,5-trialkoxybenzamide] amido or iodo benzene cores induces liquid crystalline materials. The nature of the group linking the Bodipy to the platform and the length of the aliphatic chains play a crucial role in the stabilization of the thermotropic mesophases. For the ethynyl family, the octyloxy is not mesomorphic, whereas the dodecyloxy exhibits a columnar mesophase over 5 °C and the hexadecyloxy compound exhibits mesomorphism over 30 °C. The analogous amide compounds are mesomorphic at higher temperature due to additional stabilization via hydrogen bonding of the third amide function, and the mesophase domain extends over a larger temperature domain (over 70 °C). The bright green luminescence of ordered Bodipy mesophases is maintained and easily observed by a fluorescence microscope. This is an important observation that can adequately demonstrate that the homogeneity and the quality of luminescent thin films can be checked by fluorescence microscopy.

Based on the crystal structure of a B^{1}amide derivative, we suggest that the columnar mesophase is likely driven by formation of a dimer stabilized by hydrogen bonding. In all cases, the amide functions are engaged in a supramolecular hydrogen-bonded network, as confirmed by infrared studies. A remarkable feature of the tris-amide derivative with $n = 16$ is the gelation of nonane. Fluorescence measurements on the robust gels show that the emission originates from eximers and excited oligomers as deduced from temperature variable steady-state fluorescence measurements. The different techniques used showed that the formation of gels originates from a combination of hydrogen bonds and fluorophores interactions, but the fluorophore aggregation is the main driving force that controls the formation of the gel. Formation of ordered Bodipy containing mesophases provides a facile route to prepare nanostructured films in which the fluorescence properties are controlled by the degree of aggregation. Tuning the color of the gel, mesophases and films are feasible by changing the extension of electronic delocalization within the cyanine core, and reasonable emission is envisioned from green to red. Work along these lines is currently in progress in our laboratory.

Acknowledgment. This work was supported by the University Louis Pasteur (ULP), the School of Chemical Engineering (ECPM), and the CNRS. Dr. Benoît Heinrich is gratefully acknowledged for his skilled assistance in the FTIR measurements. Dr. Marc Schmutz (ICS, CNRS−UPR 22, Strasbourg) is also acknowledged for the electron microscopy experiments.

Supporting Information Available: Complete experimental section including description of the equipment, preparation and characterization of the compounds, X-ray crystal data and treatments, molecular packing, DSC traces, solid-state emission, luminescence textures, TEM and FFEM analysis. This material is available free of charge via the Internet at http://pubs.acs.org.

CM0611441